An Effective Approach for Rotor Electrical Asymmetry Detection in Wind Turbine DFIGs

Raed Khalaf Ibrahim, Simon J. Watson, *Member, IEEE*, Siniša Djurović, and Christopher J. Crabtree

***Abstract*—Determining the magnitude of particular fault signature components (FSCs) generated by wind turbine (WT) faults from current signals has been used as an effective way to detect early abnormalities. However, the WT current signals are time varying due to the constantly varying generator speed. The WT frequently operates with the generator close to the synchronous speed, resulting in FSCs manifesting themselves in the vicinity of the supply frequency and its harmonics, making their detection more challenging. To address this challenge, the detection of rotor electrical asymmetry in WT doubly fed induction generators, indicative of common winding, brush gear, or high resistance connection faults, has been investigated using a test rig under three different driving conditions, and then an effective extended Kalman filter (EKF) based method is proposed to iteratively estimate the FSCs and track their magnitudes. The proposed approach has been compared with a continuous wavelet transform (CWT) and an iterative localized discrete Fourier-transform (IDFT). The experimental results demonstrate that the CWT and IDFT algorithms fail to track the FSCs at low load operation near-synchronous speed. In contrast, the EKF was more successful in tracking the FSCs magnitude in all operating conditions, unambiguously determining the severity of the faults over time and providing significant gains in both computational efficiency and accuracy of fault diagnosis.**

***Index Terms*—Condition monitoring (CM), continuous wavelet transform (CWT), doubly fed induction generators (DFIGs), extended Kalman filter (EKF), fault diagnosis, Fourier transform, induction generators, signal processing, time-frequency analysis, wavelet transforms, wind power generation, wind turbines (WTs).**

Manuscript received September 5, 2017; revised November 29, 2017 and January 17, 2018; accepted February 13, 2018. Date of publication March 19, 2018; date of current version June 26, 2018. This work was supported by the SUPERGEN Wind Hub under Grant EP/L014106/1. The work of R. K. Ibrahim was supported by the Higher Committee for Education Development in Iraq. *(Corresponding author: Raed Khalaf Ibrahim.)*

R. K. Ibrahim is with the Wolfson School of Mechanical, Electrical and Manufacturing Engineering, Centre for Renewable Energy Systems Technology, Loughborough University, Loughborough LE11 3TU, U.K. (e-mail: r.ibrahim@lboro.ac.uk).

S. J. Watson is with the TU Delft Wind Energy Institute, Delft University of Technology, Delft 2629 HS, The Netherlands (e-mail: s.j.watson@tudelft.nl).

S. Djurović is with the School of Electrical and Electronic Engineering, Manchester University, Manchester M13 9PL, U.K. (e-mail: sinisa.durovic@manchester.ac.uk).

C. J. Crabtree is with the School of Engineering, Durham University, Durham DH1 3HP, U.K. (e-mail: c.j.crabtree@durham.ac.uk).

Color versions of one or more of the figures in this paper are available online at http://ieeexplore.ieee.org.

Digital Object Identifier 10.1109/TIE.2018.2811373

I. Introduction

In RECENT years, wind energy has experienced substantial growth compared to other forms of power generation. While alternatives are emerging, a large proportion of currently installed and manufactured wind turbines (WTs) continue to use induction generators. The doubly fed induction generator (DFIG) in particular remains an attractive generator technology with a strong market position [1] due to its unique wide-range variable-speed-constant-frequency operating capability coupled with low-power electronic inverter rating requirements and effective power flow control.

Undetected generator faults in DFIGs have been associated with high failure rates, replacement of major components, and subsequent significant downtime [2]. The primary cause of this higher downtime in the offshore environment is the increased need for heavy-lifting vessels [3]. Usually, faults evolve from an incipient stage to a progressively more severe condition and eventually turn to failure. Early fault detection can hence avoid catastrophic failures and downtime reduction through enabling careful condition-based maintenance planning [4]. An analysis of failure statistics showed that 20% to 70% of the generator faults were related to bearings, 3% to 38% to the stator, 7% to 50% to the rotor, and the rest were categorized as "other" [5]. Another study, which reviewed 80 journal papers published by the IEEE and IEE/IET on the subject of induction machine failure statistics over the past 26 years, reported that 21% of generator faults were bearing problems, 35% stator related, and 44% rotor related [6]. Rotor electrical unbalance is identified as an indicator of some of the major contributors to WT generator failure rate [7], [8]. This condition is representative of a number of recognized rotor electrical fault modes in DFIG systems such as brush gear degradation, rotor winding fault, and/or improper connection between the slip ring unit and the rotor cable leads and its analysis and detection have been the topic of a number of studies conducted on representative academic scale test rig systems and MW-size DFIG field applications [4]–[12]. Undetected electric faults may gradually develop to a major short circuit, and can cause severe damage to the machine and the system to which it is connected [13]. Therefore, early detection of rotor electrical unbalance faults of in-service generators is essential to eliminate consequential damage.

Previous works [14], [15] showed that faults in electrical machines can be detected in a noninvasive manner by either current or power signal analysis. The use of current and power signals analysis has consequently been proposed as a general tool for

WT fault detection [16]–[20]. In particular, the diagnostic application of stator current signature analysis to detect DFIG rotor asymmetry conditions has been studied on laboratory test rigs, simulation studies [5], [8], [9], [21], [22], or analytical formulations of fault frequencies [10], [11]. Rotor electrical unbalance has been emulated by connecting external resistances to machine windings [4]–[11], [23], [24].

The available literature indicates that rotor asymmetries generate particular spectral signatures (called fault signatures) in the frequency spectra of WT current signals. Theoretical and analytical formulations of fault signature frequencies and their generation were attempted in [8], [10], and [25] to define the signal spectral component that can be monitored for diagnostic purposes. To date, various WT condition monitoring (CM) techniques that aim to utilize these and similar diagnostic signals have been developed [17], [19], [26], [27]. However, a fully satisfactory method to detect the full range of WT faults in their early stages has not been achieved yet, and false alarms are still frequently reported from sites with the generator being a significant contributor [2], demonstrating the need to optimize these alarms. The root cause of generator false alarms can be related to the following problems.

1) The lack of clear understanding of the diagnostic information embedded in the DFIG stator current spectral content.
2) The lack of signal processing tools with sufficient sensitivity and reasonable computational efficiency to extract the instantaneous amplitude (IA) of fault signature components (FSCs) from the WT current signals.

The first problem has largely been addressed in [9], [10], [21], and [28] with a comprehensive theoretical analysis of the DFIG stator current spectrum content for the machine operating in steady state, both with and without supply and/or winding asymmetries. The research reported in this paper will focus on a potential solution to address the second problem where the FSCs in the WT current signals have nonlinear and nonstationary characteristics due to the constantly varying shaft rotating speeds caused by turbine variable loads [29]. Furthermore, a wide range of CM technique performance assessment under relevant transient conditions has not been widely reported in the literature, particularly when the machine operates at low load near to synchronous speed. As a result, in these conditions, the FSCs are particularly difficult to detect or differentiate using existing methods, which may lead to an increase in the false alarms for these conditions. This problem has not received attention in reported literature despite the fact that actual WTs frequently operate at low load conditions where the generator rotational speed is close to the synchronous speed, motivating the research in this study to propose potential solutions.

In this paper, we introduce an effective approach to enhance the detection of rotor electrical asymmetry in WT DFIGs by analyzing the generator current signals. First, the analytical expressions defining rotor electrical asymmetry fault signature in DFIG stator current described in [9] and [28] have been used to enable FSCs to be recalculated over time as a function of machine speed. Second, an adaptive extended Kalman filter (EKF) tracker has been proposed to extract the IAs of the FSCs based on the corresponding machine speed signal and the estimated error covariance. At each time step, the calculated FSCs along with those extracted from the measured current signal are processed by the EKF to predict the future state of the FSCs, and continuously update the IAs of FSCs as real-time monitored signal data samples become available. The proposed technique has been validated experimentally on a WT drive train test rig with two fault levels of rotor electrical asymmetries at three different driving conditions whose variability is representative of WT generator field operation. The performance of the proposed approach is compared with some of the leading WT generator CM techniques [9], [30]. The reported experimental findings demonstrate clear and significant gains in both the computational efficiency and the diagnosis accuracy using the proposed technique.

This paper is organized as follows. Section II describes the signature of rotor electrical asymmetry in the DFIG current signals and the use of continuous wavelet transform (CWT) and iterative localized discrete Fourier-transform (IDFT) for frequency tracking. Section III describes the methodology used in the present work using an EKF for diagnosing rotor electrical asymmetry. Section IV describes the data available and employed in this paper. In Section V, the results obtained for three test cases are presented using the EKF, CWT, and IDFT tracking algorithms. Finally, conclusions are drawn and final remarks are made in Section VI.

II. Frequency Tracking and Fault Detection

The rotor electrical asymmetry condition in DFIGs is manifested through a range of additional sideband components in the stator current signal spectrum; it was experimentally proven in [9] and [28] that the rotor electrical imbalance faults in a WT-based DFIG can give rise to additional frequency components in the stator current at frequencies given by

$$f_f = \left(I \pm \frac{k(1-s)}{p} \right) . f_s \tag{1}$$

where f_f are the series of the calculated FSCs related to the fault, f_s is the fundamental supply frequency, k is the component order ($k = 1, 2, 3, ...$), s is the slip, I is a constant that relates to air-gap field space harmonics, and p is the number of pole pairs.

Rotor electrical imbalance faults could be detected by monitoring the magnitudes of the components in (1) over time, taking into account variable operating conditions. Efforts have been made to extract the magnitude of the FSCs using a CWT [31]–[33]. However, the CWT cannot achieve fine resolution in both the time and frequency domains simultaneously. In addition, high computational time (CT) is needed to obtain good results with the CWT, making it unsuitable for large size data analysis. To overcome this, another frequency tracking methodology was proposed in [9] using the IDFT algorithm to extract the energy of the FSCs, defined in (1), over time. The IDFT has good computational efficiency and applies a discrete Fourier analysis over a narrow band around the frequency of interest to extract a peak amplitude, which is assumed to be the amplitude of the FSC within the predefined window. However, the challenge with this

assumption is that the FSC can be difficult to isolate accurately as it can be merged with other frequency components irrelevant to the fault or it can be hidden in other components such as the supply frequency and its harmonics due to the variable operating conditions. This makes the use of the IDFT difficult to implement when monitoring actual WTs. One of the purposes of this paper is to demonstrate an approach, which is better able to isolate an FSC under variable loading conditions. Section III will illustrate the theory behind this approach.

III. EKF for Frequency Tracking

The EKF is an efficient recursive algorithm widely applied in the fields of radar tracking [34] and adaptive control [35]. The conventional Kalman filter assumes a linear system dynamics model with Gaussian noise in the measurements, which is not always realistic in many applications. The EKF on the other hand is an extension of the conventional Kalman filter to nonlinear system dynamics and has been used for state estimations of induction motors and WT DFIGs [36], [37]. In this section, the observed FSC at time k is first modeled. The mathematical formulation of the EKF used to iteratively estimate the FSCs is then briefly presented. Theoretically, the stator current waveform in one phase (e.g., phase A) of DFIG can be expressed as follows:

$$\boldsymbol{z}_k(t) = \sum_i A_i \cos(2\pi f_i t_k + \theta_i) \tag{2}$$

where A_i and f_i are the amplitude with initial phase θ_i and the frequency of the ith sinusoid, respectively. We used a Fourier transform to convert the time description of the stator current waveform into an equivalent function in the frequency domain thus

$$\boldsymbol{z}_k(f) = \sum_i A_i[\delta(f_k + f_i) + \delta(f_k - f_i)]. \tag{3}$$

The one-sided Fourier transform of (3) at (f_s) the main supply frequency can be written as follows:

$$\boldsymbol{z}_k(f) = A\delta(f_k - f_s). \tag{4}$$

By substituting (1) into (4), we obtain the representation of the FSCs in the frequency domain

$$\begin{aligned}\boldsymbol{z}_k(f) &= A\delta\left(f_k - \left(\frac{p}{pI \pm k(1-s)}\right) f_f\right) \\ &= A\delta(f_k - \alpha f_f)\end{aligned} \tag{5}$$

where

$$\alpha = \left(\frac{p}{pI \pm k(1-s)}\right). \tag{6}$$

The dynamics of the state variables can be represented by the state variable equation as follows:

$$\boldsymbol{x}_k = \mathbf{f}(\boldsymbol{x}_{k-1}, \mathbf{u}_k) + \mathbf{w}_k \tag{7}$$

where $\mathbf{f}$ is a nonlinear function of states, $\mathbf{u}_k$ is the control vector, and $\mathbf{w}_k$ is a white noise driving function to account for the dynamic variation of the state variables. The observed FSC $\boldsymbol{y}_k$ at time k with the additive noise $\boldsymbol{v}_k$ can be described as follows:

$$\boldsymbol{y}_k = \mathbf{z}_k + \mathbf{v}_k \tag{8}$$

and can be represented by the following linear stochastic system:

$$\boldsymbol{y}_k = \begin{bmatrix} 1 & 1 \end{bmatrix} \begin{bmatrix} A \\ \alpha f_f \end{bmatrix} + \mathbf{v}_k. \tag{9}$$

The above-mentioned linear representation is also equivalent to the following nonlinear stochastic system:

$$\text{State equation } \boldsymbol{x}_{k+1} = \mathbf{f}(x_k) + \mathbf{w}_k \tag{10}$$

$$\text{Measurement equation } \boldsymbol{y}_k = \mathbf{H}\boldsymbol{x}_k + \mathbf{v}_k \tag{11}$$

where

$$\boldsymbol{x}_k = \begin{bmatrix} x_k(1) & x_k(2) \end{bmatrix}^T = \begin{bmatrix} A & \alpha f_f \end{bmatrix}^T \tag{12}$$

$$\mathbf{f}(x_k) = \begin{bmatrix} x_k(1) & x_k(1)x_k(2) \end{bmatrix}^T = \begin{bmatrix} A & A\alpha f_f \end{bmatrix}^T \tag{13}$$

$$\boldsymbol{H} = \begin{bmatrix} 1 & 1 \end{bmatrix}. \tag{14}$$

This formulation leads to the EKF algorithm in order to linearize the above-mentioned system, which is slightly different from a standard linear Kalman filter model. The recursive tracking process of a series of fault frequencies at any time step from k equal to zero is outlined as follows.

Step 1: Predict the estimates of the state variables $\hat{\boldsymbol{x}}_{k+1|k}$ and the error covariance $\mathbf{M}_{k+1|k}$

$$\hat{\boldsymbol{x}}_{k+1|k} = \mathbf{f}\hat{\boldsymbol{x}}_{k|k} \tag{15}$$

$$\mathbf{M}_{k+1|k} = \mathbf{F}\mathbf{P}_{k|k}\mathbf{F}^T + \mathbf{Q}_k. \tag{16}$$

Step 2: Update the Kalman gain $\mathbf{K}_k$

$$r_k = |\boldsymbol{z}_k - \hat{\boldsymbol{z}}_k| \tag{17}$$

$$\mathbf{S}_k = \mathbf{H}_k\mathbf{P}_{k|k-1}\mathbf{H}_k^T + r_k \tag{18}$$

$$\mathbf{K}_k = \mathbf{P}_{k|k-1}\mathbf{H}_k^T\mathbf{S}_k^{-1} \tag{19}$$

where

$$\begin{aligned}\mathbf{F}_k &= \frac{\partial \mathbf{f}(x_k)}{\partial x_k}\Big|_{x_k = \hat{x}_{k|k}} = \begin{bmatrix} 1 & 0 \\ \hat{x}_{k|k}(2) & \hat{x}_{k|k}(1) \end{bmatrix} \\ &= \begin{bmatrix} 1 & 0 \\ (1-\varepsilon)(\alpha\hat{f}_f)_{k|k} & \hat{A}_{k|k} \end{bmatrix}.\end{aligned} \tag{20}$$

Step 3: Update the state variables $\hat{\boldsymbol{x}}_{k|k}$

$$\hat{\boldsymbol{x}}_{k|k} = \bar{\boldsymbol{x}}_{k|k-1} + \mathbf{K}_k[\boldsymbol{y}_k - \mathbf{H}_k(\bar{\boldsymbol{x}}_{k|k-1})]. \tag{21}$$

Step 4: Update the error covariance

$$\begin{aligned}\mathbf{P}_{k|k} &= (\mathbf{I} - \mathbf{K}_k\mathbf{H})\mathbf{P}_{k|k-1} + q\mathbf{B} \\ \mathbf{B} &= \begin{bmatrix} 0 & 0 \\ 0 & 1 \end{bmatrix}\end{aligned} \tag{22}$$

where the symbols $\bar{}$ and $\hat{}$ stand for the predicted and updated values, respectively. $\mathbf{I}$ is the identity matrix. The vector $\boldsymbol{z}_k$ is the observed FSCs, which is obtained by applying the fast Fourier transform (FFT) algorithm for each interval of interest from the current signal in the time domain, and $\hat{\boldsymbol{z}}_k$ is the expected normal

state, which represents the calculated FSCs in (1). r_k denotes the measurement innovation.

The design of a stable EKF was largely addressed in [38] and [39], which reports theoretically supported design guidelines to characterize the EKF design by a vector of three parameters (r, ε, q). An easier and more transparent tuning of EKFs is introduced in [40] where the results showed that ε must be set to zero to achieve the basic property of unbiasedness, and that the performance of the EKF tracker then only depends on the ratio $\lambda = r/q$; Bittanti and Savaresi [40] proceed to suggest that $q = 1$ (and hence $\lambda = r$) for a further significant simplification of the tuning procedure. Hence, the task of tuning the design parameters of the EKF tracker (parameterized with r, ε, q) is reduced to the fact that only a single parameter ($\lambda = r$) has to be chosen [40]. This EKF tuning approach was followed in this paper, where r is set to be the difference between the observed FSCs and the calculated FSCs in order to limit the variation of the innovation vector, cope with spurious measured values, enhance the estimated accuracy, and help the EKF to provide proper weighting.

In the implementation of the EKF, we assume that at time k an initial estimate of the state variable is known and is denoted by $\boldsymbol{x}_{k-1|k-1}$ and that its associated covariance matrix is also known and denoted by $\mathbf{M}_{k-1|k-1}$. The estimated variables are not affected by this assumption because the EKF is not sensitive to moderate changes in the initial covariance [41].

The principal stages of the tracking method based on the EKF to iteratively estimate the FSCs in the stator current signal are as follows.

1) Input the initial measured generator rotational speed and the stator current data points, the initial value of the state variables $\boldsymbol{x}_0$ and its associated covariance matrix $\mathbf{M}_0$, and covariance of the measured error r_0 at a sampling interval Δt_k.
2) Calculate the mean speed for the sample and the slip.
3) Calculate the stator current spectrum using an FFT.
4) Calculate discrete constants from frequencies of interest, k.
5) Calculate amplitudes for each constant, k.
6) Extract maximum amplitude and its frequency $\boldsymbol{z}_k$.
7) Calculate the FSCs of interest using (1) $\hat{\boldsymbol{z}}_k$.
8) Predict the estimates of the state variables and the error covariance using (15) and (16).
9) Calculate covariance of the measured error r_k using (17).
10) Compute the Kalman filter gain $\mathbf{K}_k$ using (19).
11) Update the estimates of the state variables and the error covariance with the measurement $\boldsymbol{z}_k$ using (21) and (22).
12) Project ahead using (15) and (16).
13) Repeat the process starting with next sampling interval Δt_{k+1}.

IV. Case Study

The proposed approach has been applied to the generator current signals collected from a purpose built WT drive train test rig. As shown in Fig. 1, the test rig comprises a 54-kW dc variable-speed drive connected via a two-stage gearbox to a four-pole DFIG that was rated for the experiment at 30 kW. The rotational speed of the dc motor is controlled by an external model incorporating the properties of a 2-MW WT operating under closed-loop conditions, driven by realistic wind conditions at a variety of wind speeds and turbulence intensities. The rotor circuit of the generator is coupled via slip rings to an external three-phase resistive load bank so that electrical imbalance can be applied to the generator rotor. The test rig was instrumented and controlled using LabVIEW, see [42] for more details. In the experiments, a rotor unbalance fault was implemented on the test rig by adding two additional external resistances to one phase of the rotor circuit through an external load bank. In the healthy state, the rotor resistance was 1.3 Ω per phase and additional resistances of 0.3 and 0.6 Ω were successively added to one phase to create two fault levels. These correspond to two levels of rotor unbalance of 23% and 46%, respectively, given as a percentage of the rotor balanced phase resistance. The test rig enables the generator to be driven at a desired preprogramed wind speed profile that emulates realistic WT transient behavior and is achieved by providing a predefined speed reference profile to the controller. The relevant signals for CM were collected from the terminals of the generator at a sampling frequency of 5 kHz. An example of the measured current signal under faulty conditions is shown in Fig. 2.

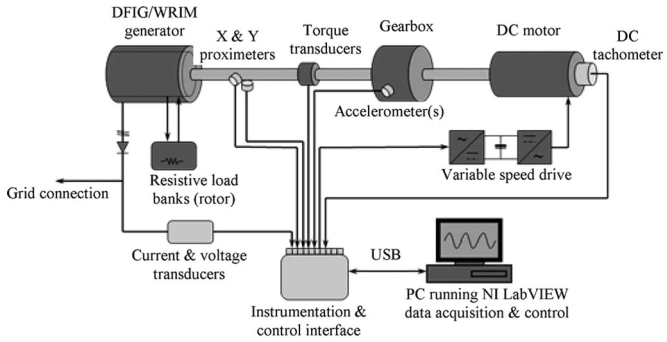

Fig. 1. Schematic representation of the test rig.

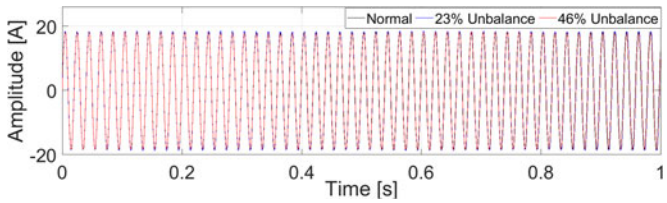

Fig. 2. Current–time waveform.

It can be seen that the amplitude of the current–time waveform gave no indication of abnormal conditions. Consequently, an FFT algorithm is used to convert the generator current signal from the time domain into the frequency domain in a healthy condition (no unbalance) and with a rotor unbalance, as shown in Fig. 3. As is generally expected for any grid connected machine the supply frequency (50 Hz) and its harmonics are clearly seen in the spectra. There are also spectral components present

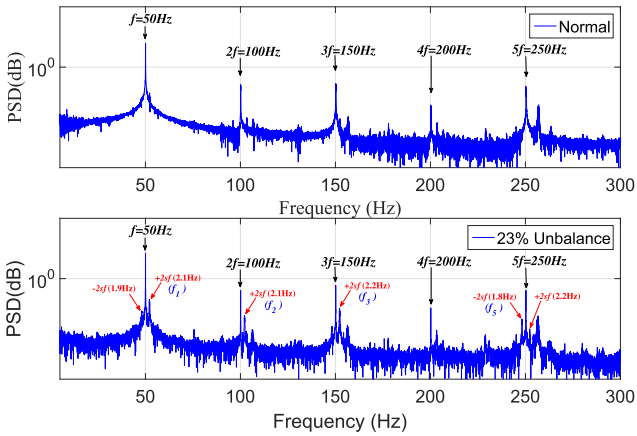

Fig. 3. Comparison of the current spectra for healthy case and rotor unbalance case.

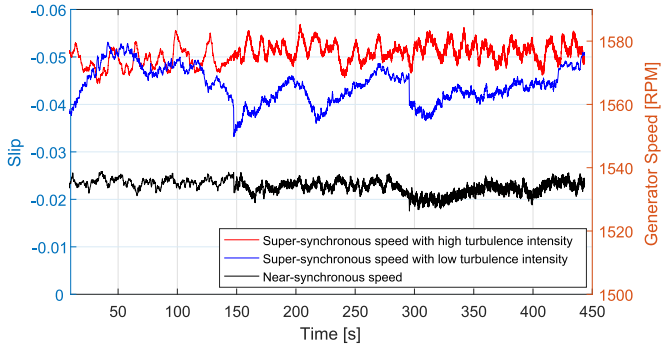

Fig. 4. Generator speed test conditions.

around the even and odd harmonics even when operating in a healthy state. This is believed to be caused by pre-existing low-level rotor excitation imbalance commonly induced by inherent manufacturing imperfections [9], [21]. However, the comparison of healthy and faulty data indicates a significant rise in the magnitude of a number of twice slip frequency 2sf sideband components on the current harmonics, which can be clearly observed when the 23% unbalance is applied to the generator rotor. In Fig. 3, the FFT algorithm cannot reveal the time information of any frequency changes, i.e., no time-domain information is available regarding fault occurrence and progression. Thus, an EKF has been proposed to detect faults by monitoring the magnitudes of the FSCs over time, taking into account variable operating conditions. The rotor unbalance fault gave rise to a number of side-band components in the current spectra. Monitoring all components would be impractical in an operating environment, so we have selected a series of FSCs that exhibit the highest magnitude. The FSCs of interest to be tracked using the EKF algorithm are labeled as f_1, f_2, f_3, f_5 in Fig. 3.

V. Performance Comparison

In order to show the effectiveness of the proposed approach based on an EKF, we have selected the CWT and IDFT, used in [9] and [30] for WT generator CM, for comparison. The algorithms are tested under varying rotational speed conditions representative of the operating regimes seen by a hypothetical WT out in the field. At each test, the test rig was run for a period of 150 s after which the 23% and 46% unbalance fault conditions were applied at 150 s and 300 s, respectively. The driving conditions selected for testing are shown in Fig. 4, corresponding to the following WT operating conditions.

Test case 1. Supersynchronous speed with high turbulence intensity: In this test, a high mean wind speed (15 m/s) with high turbulence intensity (20%) was applied to the test rig via a dc motor, the speed of which was controlled by an external model incorporating the properties of a 2-MW exemplar turbine model developed by the University of Strathclyde as part of the Supergen Wind Energy Technologies Consortium [9]. The CWT, IDFT, and EKF methods have been applied to the current spectra in Fig. 3 to extract the IAs of the four defined frequencies of interest (f_1, f_2, f_3, f_5) for the detection of rotor unbalance. The results under supersynchronous speed with high turbulence intensity are shown in Fig. 5. Note, if the tracked FSC of each method shows a step change in magnitude when the fault condition was present or has changed, then the method has successfully captured the component frequency related to the fault.

In Fig. 5(a), the conventional CWT is able to capture fault components f_1 and f_2 where their IAs did show a marked change when the fault condition was applied or has changed. The CWT failed to capture other components due to the influence of the window function on the results, where the window size is well matched with the oscillation of component f_1 and f_2 but as the fault frequency increases the window is no longer able to capture the variation of the fault components. A more robust window design is necessary in order to improve simultaneously high time resolution and high frequency resolution. But, this is not an easy task as the difference between the f_1, f_2, and f_3 components is about 50 Hz and increases to 100 Hz for component f_5. In addition, these components overlap with the main supply frequencies and other dominant frequency components of the current signal that are irrelevant to the fault. To overcome these shortcomings, the IDFT algorithm was applied to extract the magnitude of the FSCs. The results are shown in Fig. 5(b).

In Fig. 5(b), it is seen that the IDFT method has successfully tracked the magnitude of the four fault-related frequencies with increasing fault severity (i.e., from 300 to 450 s) despite the fact that the shaft speed was varying continuously throughout the experiments. Similar to the IDFT results, the EKF algorithm has successfully picked up the four FSCs that are changing proportionally to the rotational speed, as shown in Fig. 5(c). The results show that the EKF is able to track the fault frequencies, giving quantitative information about the fault progression.

However, the tracking results of each algorithm in Fig. 5 follow different variation tendencies due to the fact that the current signals from an operational WT are not stationary but are time varying in nature because of the constantly varying generator speed, making the detection of FSCs by the tracking algorithms more challenging. In order to demonstrate the best achieved performance for detecting the rotor unbalance fault and revealing the actual fault degree, the performance of all diagnostic methods during the fault event is evaluated using root-mean-squared error (RMSE) values. Since the increase in the degree of rotor unbalance can be calculated from the IA

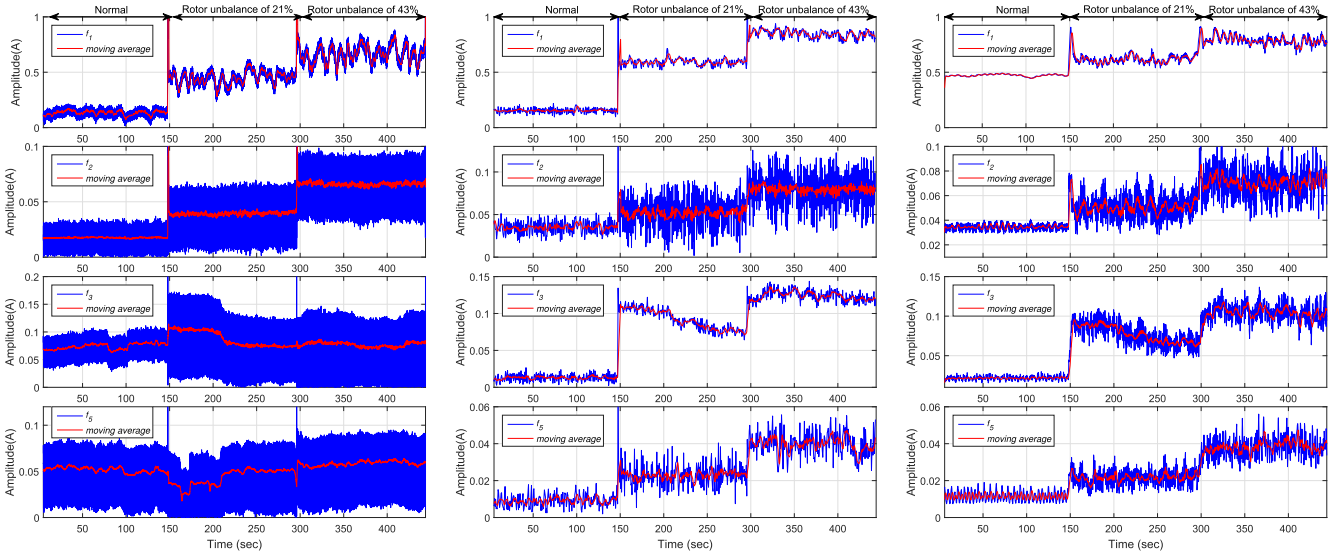

Fig. 5. Tracking the magnitude of fault frequencies of interest using (a) CWT, (b) IDFT, and (c) EKF for test case 1.

TABLE I
RMSE OF THE TRACKING METHODS FOR TEST CASE 1

FSCs	RMSE values (%)		
	CWT	IDFT	EKF
f_1	1.967	2.135	0.325
f_2	1.134	1.301	0.258
f_3	N/A	2.115	0.441
f_5	N/A	0.420	0.236

TABLE II
RMSE OF THE TRACKING METHODS FOR TEST CASE 2

FSCs	RMSE Values (%)		
	CWT	IDFT	EKF
f_1	2.757	2.413	0.318
f_2	2.213	0.608	0.276
f_3	N/A	2.067	0.382
f_5	N/A	0.388	0.234

variations of the FSCs extracted by the diagnostic methods, a general expression is derived for machine operation with rotor unbalance degree $\hat{\boldsymbol{\eta}}_k$ by calculating the difference between the IA for each component under healthy and faulty conditions divided by the order of the component order times the average under healthy conditions as follows:

$$\hat{\boldsymbol{\eta}}_k = \frac{\mathbf{IA}_f - \mathbf{IA}_h}{\mathbf{k}.\mathbf{IA}_h} \times 100\% \tag{23}$$

where $\mathbf{IA}_h$ and $\mathbf{IA}_f$ are the IA at any time step k for each component under healthy and faulty conditions, respectively, and $\mathbf{k}$ is the component order ($\mathbf{k} = 1, 2, 3, ...$). The RMSE is given by

$$\mathbf{RMSE} = \frac{1}{N}\sum_{i=1}^{N}(\boldsymbol{\eta}_i - \hat{\boldsymbol{\eta}}_i) \tag{24}$$

where $\boldsymbol{\eta}_i$ is the degree of the fault during the experiment, corresponding to the two levels of rotor unbalance of 23% and 46%. Table I summarizes the results of the performance evaluation. It is clear from the table that the IDFT and EKF methods perform best in terms of the RMSE for all FSCs. The CWT is incapable of detecting the fault by tracking the components f_3 and f_5, but the RMSE values for components f_1 and f_2 are lower than the same components for the IDFT. The comparison between the three methods shows that the RMSE for all FSCs is much lower when using the EKF method.

Test case 2. Supersynchronous speed with low turbulence intensity: This test represents 7.5 m/s mean wind speed with low turbulence intensity 6%. The slip for this state differs significantly from case 1 with a wide range as seen in Fig. 4. Similar results to the previous test case are observed in Fig. 6, where the CWT is only able to track the fault component f_1 and f_2. This explains why in [30] and [43] only the fault component f_1, which is the twice slip frequency was tracked using the CWT. In contrast, both the IDFT and EKF methods can successfully show the presence of the fault. It is also clear that the variation tendencies of the IAs at the four characteristic frequencies have been correctly extracted despite the time-varying features due to the variable-speed operation and the disturbance of the components unrelated to the fault.

The performances of the three methods are summarized in Table II. Again, the performance of the IDFT and EKF is better in terms of the RMSE values for all FSCs. Compared to the CWT and IDFT, the EKF proved capable of dealing with different variable-speed driving conditions with lower RMSE values. In addition, the components f_1 and f_2 for the CWT show higher RMSE values compared to the results in case 1 as larger variation

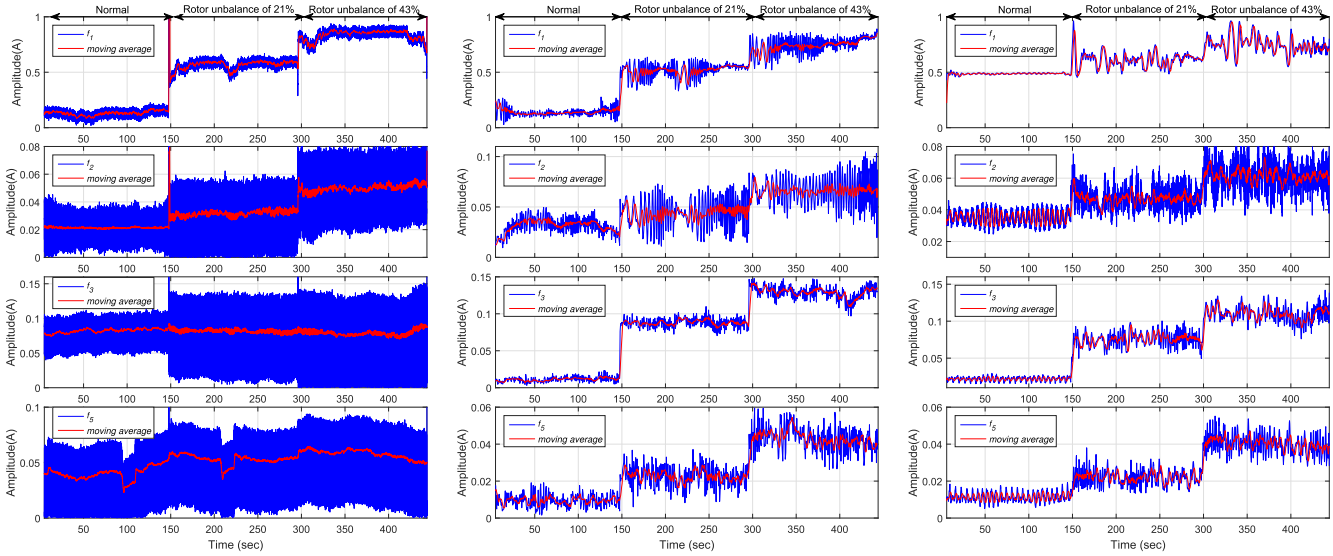

Fig. 6. Tracking the magnitude of fault frequencies of interest using (a) CWT, (b) IDFT, and (c) EKF for test case 2.

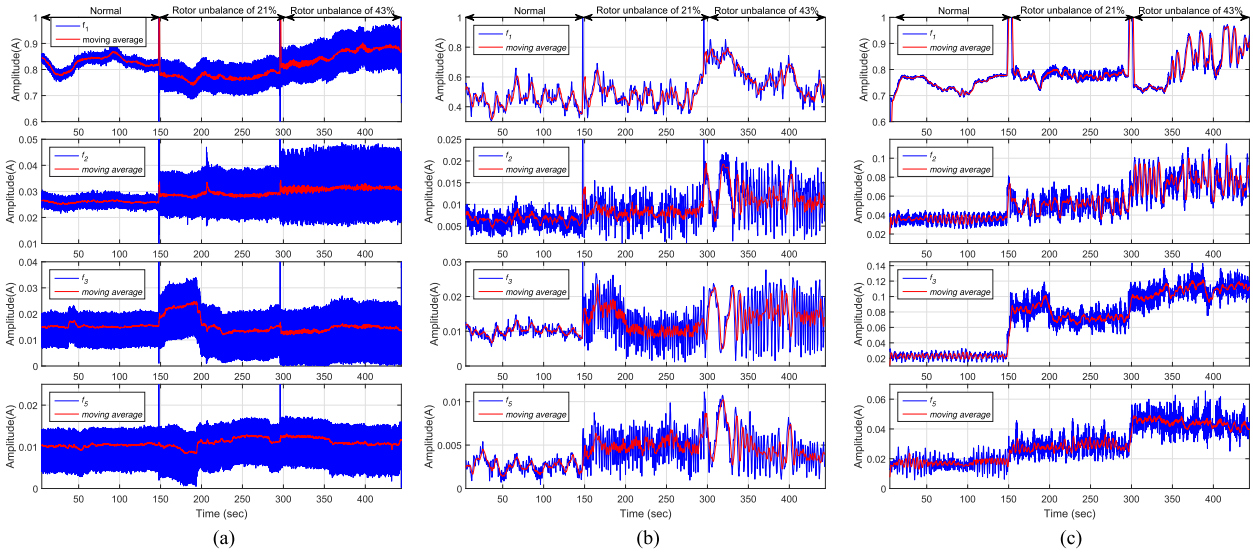

Fig. 7. Tracking the magnitude of fault frequencies of interest using (a) CWT, (b) IDFT, and (c) EKF for test case 3.

in rotational speed for test case 2 makes it more challenging to track the FSCs. It can be concluded that the EKF not only showed the best performance overall in terms of RMSE metric, but also in terms of the rotor unbalance fault detection at different driving conditions, whereas the CWT method performed worst. One explanation for the poor performance of the CWT method can be the windowing technique, which has been influenced by the speed variations.

Test case 3. Near-synchronous speed: Following the successful detection of the fault conditions at supersynchronous speed, it is important now to verify the CM capability of the algorithms when the machine operates near to the synchronous speed. In this case, the slip will be near to zero so the FSCs in (1) will be very close to the supply frequency (50 Hz) and its harmonics (both odd and even), making CM and fault detection more challenging even though this condition occurs frequently for an operational WT. The results of such a scenario are shown in Fig. 7.

Both the CWT and IDFT algorithms, shown in Fig. 7(a) and (b), have failed to effectively track the FSCs; the shortcoming of the CWT and IDFT methods is that both use windowing technique, and do not have an observer to avoid tracking the FSCs when they are so close as to be effectively merged with the supply frequency and its harmonics.

On the other hand, the EKF shows much better resolution of the varying fault conditions, as shown in Fig. 7(c). The results clearly show that the amplitude of the fault-related frequencies jumps sharply when the 23% unbalance fault is introduced at

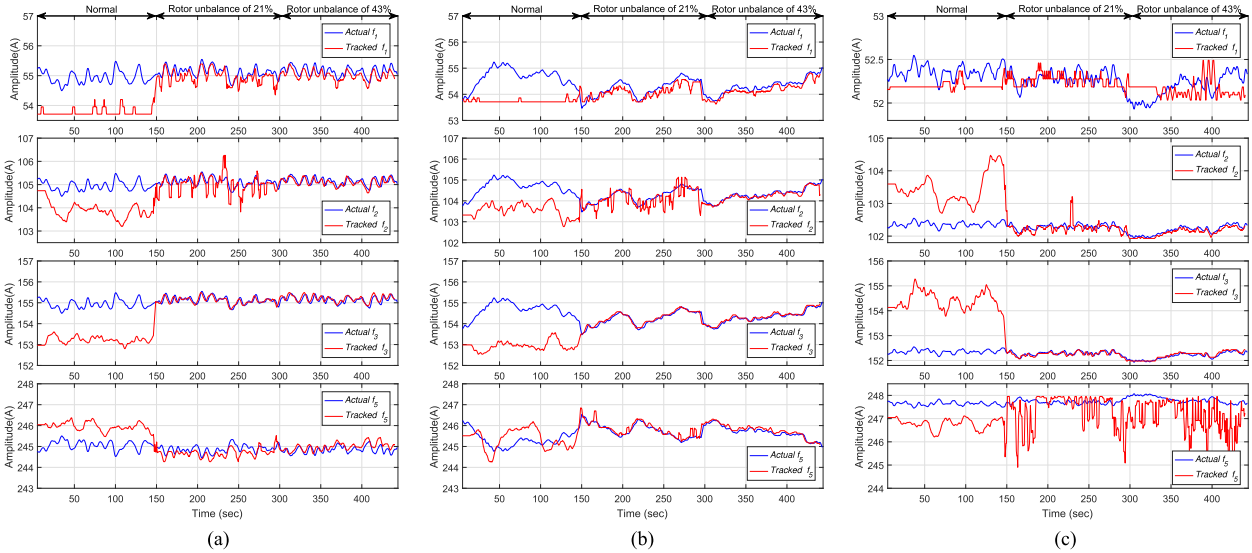

Fig. 8. Tracking the fault frequencies of interest using EKF for (a) test case 1, (b) test case 2, and (c) test case 3.

150 s. A similar jump occurs for the 46% unbalance condition introduced at 300 s that shows clear differences between healthy and faulty conditions particularly for components f_2, f_3, and f_5. The performances of the FSCs tracked by the EKF in terms of the percentage RMSE values are found to be 0.378, 0.244, 0.386, and 0.352 for f_1, f_2, f_3, and f_5, respectively. It can be seen that the EKF shows more accurate fault tracking across all the driving conditions and the RMSE values for all FSCs are very close. Over the three cases, the EKF shows better fault resolution compared to the CWT and IDFT as it does not use any windowing technique, rather it uses the Kalman gain($\mathbf{K}_k$). The Kalman gain acts as a relative weight given to the current extracted and measurement values, and its value is continuously tuned to get the correct estimation value of the FSCs and their magnitude from the nonstationary current signal. At each time step, $\mathbf{K}_k$ is calculated from the covariance. The constantly varying generator speeds and nonlinear operation lead to an increase or decrease of the Kalman gain, so with a high gain the filter places more weight on the most recent measurements, and thus follows them more responsively to avoid tracking the noise (i.e., the supply frequency and its harmonics or other dominant frequency components of the current signal), which are irrelevant to the fault. With a low gain, the filter follows the model predictions more closely to track the fault signatures and smooth out the noise.

To show the effectiveness of the proposed EKF, we compare in Fig. 8 the tracking results of the EKF associated with the spectral component frequencies against the actual frequencies, described by equation (1), across all driving conditions. As it can be seen from Fig. 8, that the tracking frequencies are different from the actual frequencies in normal operation when there is no fault because the magnitude of the actual frequencies is very small and merged with the noise so they are difficult to detect or differentiate. Once, the fault has been applied, the EKF immediately captured the frequencies related to the fault and continued to track them over time despite the fact that the actual frequencies are more affected by the speed variations and follow exactly the same speed variation tendencies, as shown in Fig. 4. It can also be seen for case 3 that the f_1 and f_5 FSCs are particularly difficult to capture compared to the others cases due to the operation at low load near to synchronous speed, resulting in FSCs manifesting themselves in the vicinity of the supply frequency and its harmonics with extraneous noise, as shown in Fig. 3. This led to an increase in the variation of the innovation vector r_k for these conditions. However, the magnitude of the tracked f_1 and f_5 FSCs is still useful for fault detection, and did show a step change in magnitude when the fault condition was present or was changed as discussed previously.

In summary, the results for the three cases show that the rotor electrical unbalance fault can be accurately detected by tracking any component using the EKF, but overall the second component f_2 showed the lowest RMSE in revealing the fault degree. The results using the IDFT in Tables I and II show that the fifth component f_5 provides the lowest RMSE (0.404 as an average percentage), whereas the results obtained from other components are not effective in revealing the degree of rotor unbalance. If we only consider component f_5 for fault diagnosis, our proposed approach demonstrates a significant improvement over the IDFT method in imbalance diagnosis accuracy by reducing the percentage RMSE from 0.404 to 0.235. Since the results show that the second component f_2 has the best accuracy in the case of the EKF, whereas the fifth component f_5 provides the best accuracy in the case of the IDFT, this indicates we have successfully reduced the volume of data required for analysis and storage. To clarify, based on the Nyqist–Shannon sampling theorem, the data requirements to monitor component f_5 for a period of one year would enable the monitoring of component f_2 for a period of approximately two years and four months, due to the fundamental fact that f_5 is greater than f_2 and requires a higher sampling rate to capture. Hence, our approach shows success in tracking the magnitude of the FSCs and revealing the severity of the faults over time with significant

TABLE III
COMPUTATIONAL COMPLEXITY OF THE TRACKING METHODS

FSCs	CT (s)		
	CWT	IDFT	EKF
f_1	35.65	0.98	1.2
f_2	20.05	1.01	1.1
f_3	14.79	1.05	1.16
f_5	4.32	1.09	1.1

gains in both the computational efficiency and the diagnosis accuracy.

A. Computational Time

To further highlight the improvement offered by an EKF, we perform CT analysis comparing the EKF method against the CWT and IDFT methods. The calculations were performed on a computer with an Intel i7 core processor and 32.0-GB RAM.

Table III shows the plot of the averaged CT for the results obtained in Figs. 5–7 for the series of FSCs. It is seen that the CWT method requires a higher CT for the FSCs with lower frequencies because these tend to have much longer wavelengths with a high signal-to-noise ratio, whereas the higher FSCs have much shorter wavelengths with low signal-to-noise ratio. Accordingly, this affects the width of the window function in time to capture the frequencies of interest; therefore, it requires more computational resources. In contrast, the IDFT and EKF require far less computational resource compared to the CWT. This is due to the fact that the IDFT and EKF methods apply a discrete Fourier analysis over a narrow band around the frequency of interest. The IDFT and EKF have very similar CT requirements making them more suitable for online monitoring than the CWT.

VI. CONCLUSION

This paper proposed the use of an EKF in the detection of rotor electrical unbalance fault, indicative of common winding, brush gear, or high resistance connection faults, in a WT DFIG. The EKF performance was compared with that of a CWT and an IDFT in terms of its ability to track a series of fault frequencies associated with three different unbalance condition levels and for three different simulated transient operating regimes using data generated by a test rig. The EKF demonstrated better overall resolution of fault frequencies particularly where those frequencies are close to the synchronous frequencies and their harmonics; a condition that can occur frequently when a turbine is operating with the generator close to synchronous speed. Due to the parsimonious nature of the EKF and the fact that it does not employ windowing, it is able to accurately detect fault frequencies with minimal computational requirements when compared with a CWT. The EKF was shown to be capable of detecting the degree of rotor unbalance with greater accuracy than an IDFT or CWT. The results presented show that the EKF algorithm shows promise as a low cost, efficient method for condition monitoring the output of a WT generator particular with regard to the detection of electrical faults such as rotor unbalance.

Future work is required to apply this approach to real operating WTs, which may be suffering from rotor electrical asymmetries, and to use the detection of the fault degree to potentially predict the fault progression some time in advance. Work is also necessary to assess the potential of the reported technique to be used for the detection of a wider range of WT faults such as generator bearing, gearbox-bearing, and rotor eccentricity faults.

REFERENCES

[1] Y. Zhou, P. Bauer, J. A. Ferreira, and J. Pierik, "Operation of grid-connected DFIG under unbalanced grid voltage condition," *IEEE Trans. Energy Conversion*, vol. 24, no. 1, pp. 240–246, Mar. 2009.

[2] Y. Qiu, Y. Feng, P. Tavner, P. Richardson, G. Erdos, and B. Chen, "Wind turbine SCADA alarm analysis for improving reliability," *Wind Energy*, vol. 15, no. 8, pp. 951–966, 2012.

[3] J. Carroll, A. McDonald, I. Dinwoodie, D. McMillan, M. Revie, and I. Lazakis, "Availability, operation and maintenance costs of offshore wind turbines with different drive train configurations," *Wind Energy*, vol. 20, no. 2, pp. 361–378, 2017.

[4] Y. Gritli, L. Zarri, C. Rossi, F. Filippetti, G. A. Capolino, and D. Casadei, "Advanced diagnosis of electrical faults in wound-rotor induction machines," *IEEE Trans. Ind. Electron.*, vol. 60, no. 9, pp. 4012–4024, Sep. 2013.

[5] M. Zaggout, P. Tavner, C. Crabtree, and L. Ran, "Detection of rotor electrical asymmetry in wind turbine doubly-fed induction generators," *IET Renewable Power Gener.*, vol. 8, no. 8, pp. 878–886, 2014.

[6] P. Tavner, "Review of condition monitoring of rotating electrical machines," *IET Elect. Power Appl.*, vol. 2, no. 4, pp. 215–247, 2008.

[7] M. Mengoni *et al.*, "Online detection of high-resistance connections in multiphase induction machines," *IEEE Trans. Power Electron.*, vol. 30, no. 8, pp. 4505–4513, Aug. 2015.

[8] Y. Gritli, C. Rossi, D. Casadei, F. Filippetti, and G. A. Capolino, "A diagnostic space vector-based index for rotor electrical fault detection in wound-rotor induction machines under speed transient," *IEEE Trans. Ind. Electron.*, vol. 64, no. 5, pp. 3892–3902, May 2017.

[9] S. Djurovic, C. J. Crabtree, P. J. Tavner, and A. Smith, "Condition monitoring of wind turbine induction generators with rotor electrical asymmetry," *IET Renewable Power Gener.*, vol. 6, no. 4, pp. 207–216, 2012.

[10] S. Williamson and S. Djurovic, "Origins of stator current spectra in DFIGs with winding faults and excitation asymmetries," in *Proc. IEEE Int. Elect. Mach. Drives Conf.*, May 2009, pp. 563–570.

[11] Y. Gritli, A. Stefani, A. Chatti, C. Rossi, and F. Filippetti, "The combined use of the instantaneous fault frequency evolution and frequency sliding for advanced rotor fault diagnosis in DFIM under time-varying condition," in *Proc. 35th Annu. Conf. IEEE Ind. Electron.*, Nov. 2009, pp. 3471–3476.

[12] G. A. Skrimpas *et al.*, "Analysis of generator bearing vibration data for diagnosing rotor circuit malfunction in DFIGs," in *Proc. Int. Conf. Elect. Mach.*, 2014, pp. 1746–1751.

[13] H. A. Toliyat, S. Choi, and S. Nandi, *Electric Machines: Modeling, Condition Monitoring, and Fault Diagnosis*. Boca Raton, FL, USA: CRC Press, 2012.

[14] M. E. H. Benbouzid, "A review of induction motors signature analysis as a medium for faults detection," *IEEE Trans. Ind. Electron.*, vol. 47, no. 5, pp. 984–993, Oct. 2000.

[15] B. Lu, Y. Li, X. Wu, and Z. Yang, "A review of recent advances in wind turbine condition monitoring and fault diagnosis," in *Proc. IEEE Power Electron. Mach. Wind Appl.*, Jun. 2009, pp. 1–7.

[16] R. K. Ibrahim and S. Watson, "Effect of power converter on condition monitoring and fault detection for wind turbine," in *Proc. 8th IET Int. Conf. Power Electron., Mach. Drives*, 2016, pp. 1–5.

[17] Z. Hameed, Y. Hong, Y. Cho, S. Ahn, and C. Song, "Condition monitoring and fault detection of wind turbines and related algorithms: A review," *Renewable Sustain. Energy Rev.*, vol. 13, no. 1, pp. 1–39, 2009.

[18] R. Ibrahim and S. Watson, "Stator winding fault diagnosis in synchronous generators for wind turbine applications," in *Proc. 5th IET Int. Conf. Renewable Power Gener.*, Sep. 2016, pp. 1–6.

[19] W. Qiao and D. Lu, "A survey on wind turbine condition monitoring and fault diagnosis—Part II: Signals and signal processing methods," *IEEE Trans. Ind. Electron.*, vol. 62, no. 10, pp. 6546–6557, Oct. 2015.

[20] R. K. Ibrahim and S. J. Watson, "Condition monitoring of permanent magnet synchronous generator for wind turbine applications," in *Proc. 3rd Conf. Control Fault-Tolerant Syst.*, Sep. 2016, pp. 648–653.
[21] S. Djurovic, S. Williamson, and A. Renfrew, "Dynamic model for doubly-fed induction generators with unbalanced excitation, both with and without winding faults," *IET Elect. Power Appl.*, vol. 3, no. 3, pp. 171–177, 2009.
[22] M. Riera-Guasp, J. A. Antonino-Daviu, and G. A. Capolino, "Advances in electrical machine, power electronic, and drive condition monitoring and fault detection: State of the art," *IEEE Trans. Ind. Electron.*, vol. 62, no. 3, pp. 1746–1759, Mar. 2015.
[23] W. Yang, P. J. Tavner, and W. Tian, "Wind turbine condition monitoring based on an improved spline-kernelled chirplet transform," *IEEE Trans. Ind. Electron.*, vol. 62, no. 10, pp. 6565–6574, Oct. 2015.
[24] P. M. de la Barrera, G. R. Bossio, and J. A. Solsona, "High-resistance connection detection in induction motor drives using signal injection," *IEEE Trans. Ind. Electron.*, vol. 61, no. 7, pp. 3563–3573, Jul. 2014.
[25] E. Artigao, A. Honrubia-Escribano, and E. Gomez-Lazaro, "Current signature analysis to monitor DFIG wind turbine generators: A case study," *Renewable Energy*, vol. 116, pt. B, pp. 5–14, Feb. 2018.
[26] R. K. Ibrahim and S. J. Watson, "Advanced algorithms for wind turbine condition monitoring and fault diagnosis," in *Proc. WindEur. Summit Conf.*, Hamburg, Germany, Sep. 2016, pp. 1–5.
[27] R. K. Ibrahim, J. Tautz-Weinert, and S. J. Watson, "Neural networks for wind turbine fault detection via current signature analysis," in *Proc. WindEur. Summit Conf.*, Hamburg, Germany, Sep. 2016, pp. 1–7.
[28] C. Crabtree, S. Djurovic, P. Tavner, and A. Smith, "Condition monitoring of a wind turbine DFIG by current or power analysis," in *Proc. 5th IET Int. Conf. Power Electron., Mach. Drives*, Apr. 2010, pp. 1–6.
[29] W. Yang, C. Little, P. J. Tavner, and R. Court, "Data-driven technique for interpreting wind turbine condition monitoring signals," *IET Renewable Power Gener.*, vol. 8, pp. 151–159, Mar. 2014.
[30] W. Yang, P. J. Tavner, C. J. Crabtree, and M. Wilkinson, "Cost-effective condition monitoring for wind turbines," *IEEE Trans. Ind. Electron.*, vol. 57, no. 1, pp. 263–271, Jan. 2010.
[31] C.-S. Tsai, C.-T. Hsieh, and S.-J. Huang, "Enhancement of damage-detection of wind turbine blades via CWT-based approaches," *IEEE Trans. Energy Convers.*, vol. 21, no. 3, pp. 776–781, Sep. 2006.
[32] C. Kar and A. Mohanty, "Monitoring gear vibrations through motor current signature analysis and wavelet transform," *Mech. Syst. Signal Process.*, vol. 20, no. 1, pp. 158–187, 2006.
[33] H. Douglas, P. Pillay, and A. K. Ziarani, "A new algorithm for transient motor current signature analysis using wavelets," *IEEE Trans. Ind. Appl.*, vol. 40, no. 5, pp. 1361–1368, Sep./Oct. 2004.
[34] G. Y. Kulikov and M. V. Kulikova, "The accurate continuous-discrete extended Kalman filter for radar tracking," *IEEE Trans. Signal Process.*, vol. 64, no. 4, pp. 948–958, Feb. 2016.
[35] F. Auger, M. Hilairet, J. M. Guerrero, E. Monmasson, T. Orlowska-Kowalska, and S. Katsura, "Industrial applications of the Kalman filter: A review," *IEEE Trans. Ind. Electron.*, vol. 60, no. 12, pp. 5458–5471, Dec. 2013.
[36] E. Zerdali and M. Barut, "The comparisons of optimized extended Kalman filters for speed-sensorless control of induction motors," *IEEE Trans. Ind. Electron.*, vol. 64, no. 6, pp. 4340–4351, Jun. 2017.
[37] S. Yu, K. Emami, T. Fernando, H. H. C. Iu, and K. P. Wong, "State estimation of doubly fed induction generator wind turbine in complex power systems," *IEEE Trans. Power Syst.*, vol. 31, no. 6, pp. 4935–4944, Nov. 2016.
[38] B. F. La Scala, R. R. Bitmead, and M. R. James, "Conditions for stability of the extended Kalman filter and their application to the frequency tracking problem," *Math. Control, Signals, Syst.*, vol. 8, no. 1, pp. 1–26, 1995.
[39] B. F. La Scala and R. R. Bitmead, "Design of an extended Kalman filter frequency tracker," *IEEE Trans. Signal Process.*, vol. 44, no. 3, pp. 739–742, Mar. 1996.
[40] S. Bittanti and S. M. Savaresi, "On the parametrization and design of an extended Kalman filter frequency tracker," *IEEE Trans. Automat. Control*, vol. 45, no. 9, pp. 1718–1724, Sep. 2000.
[41] M. Saha, R. Ghosh, and B. Goswami, "Robustness and sensitivity metrics for tuning the extended Kalman filter," *IEEE Trans. Instrum. Meas.*, vol. 63, no. 4, pp. 964–971, Apr. 2014.
[42] C. Crabtree, "Condition monitoring techniques for wind turbines," Ph.D. dissertation, Durham Univ., Durham, U.K., 2011.
[43] S. J. Watson, B. J. Xiang, W. Yang, P. J. Tavner, and C. J. Crabtree, "Condition monitoring of the power output of wind turbine generators using wavelets," *IEEE Trans. Energy Convers.*, vol. 25, no. 3, pp. 715–721, Sep. 2010.

Raed Khalaf Ibrahim received the B.Sc. degree in electrical and electronic engineering from Tikrit University, Tikrit, Iraq, in 2009, and the M.Sc. degree in electrical and electronic engineering from Mosul University, Mosul, Iraq, in 2011.

He was an Electrical Engineer with the North Oil Company and then he was selected by the Ministry of Oil to be seconded to the prestigious Baiji Oil Institute as an Industrial Teacher and a Trainer. He is currently a Ph.D. Researcher with the Centre for Renewable Energy Systems Technology, Loughborough University, Loughborough, U.K. His research interests include wind turbine condition monitoring and fault diagnosis, advanced signal processing, machine learning, artificial intelligence, and data analysis.

Simon J. Watson (M'05) received the B.Sc. degree in physics from Imperial College London, London, U.K., in 1987, and the Ph.D. degree in nuclear physics from Edinburgh University, Edinburgh, U.K., in 1990.

He has been working in the field of wind energy since 1990 and began his career with the Energy Research Unit of the Rutherford Appleton Laboratory. In 1999, he joined Good Energy, a supplier of green electricity to domestic and small commercial customers. In 2001, he was appointed as a Senior Lecturer with the Centre for Renewable Energy Systems Technology, Loughborough University, Loughborough, U.K., and in 2010, he became a Professor in Wind Energy. In 2017, he joined TU Delft as a Professor in wind energy systems and the Director of DUWIND (the TU Delft Wind Energy Institute), Delft, the Netherlands. His research interests include wind climate, wind resource assessment, wind turbine wakes and wind turbine reliability, and condition monitoring.

Siniša Djurović (M'09) received the Dipl.Ing. degree in electrical engineering from the University of Montenegro, Podgorica, Montenegro, in 2002, and the Ph.D. degree in electrical engineering from the University of Manchester, Manchester, U.K., in 2007.

He is a Senior Lecturer with the Power Conversion Group, Manchester, U.K. His research interests include electric machines and drive operation, design, monitoring and diagnostics, and their use in renewables and automotive applications.

Christopher J. Crabtree received the M.Eng. degree in engineering from Durham University, Durham, U.K., in 2007, and the Ph.D. degree in electrical engineering from Durham University, in 2011, with a thesis on condition monitoring techniques for wind turbines.

He is an Assistant Professor in Wind Energy Systems with Durham University. His research interests include reliability, condition monitoring, and operations and maintenance of offshore wind farms.

Mr. Crabtree is leading Durham's contribution to the EPSRC HOME Offshore project on wind farm reliability and operations. Much of his research has been undertaken as part of the U.K. EPSRC SUPERGEN Wind Energy Technologies Consortium.